

The Sign Problem and MEM in Lattice Field Theory with the θ Term

Masahiro Imachi^{†*)},
Yasuhiko Shinno^{◇**)} and Hiroshi Yoneyama^{◇***)}

Department of Physics, Yamagata University, Yamagata 990-8560, Japan[†]
Department of Physics, Saga University, Saga 840-8502, Japan[◇]

Lattice field theory with the θ term suffers from the sign problem. The sign problem appears as flattening of the free energy. As an alternative to the conventional method, the Fourier transform method (FTM), we apply the maximum entropy method (MEM) to Monte Carlo data obtained using the CP^3 model with the θ term. For data without flattening, we obtain the most probable images of the partition function $\hat{\mathcal{Z}}(\theta)$ with rather small errors. The results are quantitatively close to the result obtained with the FTM. Motivated by this fact, we systematically investigate flattening in terms of the MEM. Obtained images $\hat{\mathcal{Z}}(\theta)$ are consistent with the FTM for small values of θ , while the behavior of $\hat{\mathcal{Z}}(\theta)$ depends strongly on the default model for large values of θ . This behavior of $\hat{\mathcal{Z}}(\theta)$ reflects the flattening phenomenon.

§1. Introduction

In QCD and the CP^{N-1} model, topologically non-trivial configurations play important roles in determining dynamical properties and the vacuum structure. The effect of these configurations is introduced into the action with a θ term. The existence of the θ term is associated with several interesting topics, such as the strong CP problem and possible rich phase structures in θ space. It was pointed out by 't Hooft¹⁾ that a color magnetic monopole becomes a dyon-like object in regions for which $\theta \neq 0$, and this could result in the appearance of new phase structure. It was also shown in Ref. 2) that a new phase could emerge in the $Z(N)$ model. In the CP^{N-1} model, it is known that there is a first order phase transition point at $\theta = \pi$ in the strong coupling region. To obtain a comprehensive understanding of the phase structure in θ space, it is necessary to analyze the phase structure in the weak coupling region.

A numerical simulation based upon the importance sampling method is one of the most promising tools to study non-perturbative properties of field theories. This method, however, is confronted with difficulties in the case of theories possessing the θ term, because this term causes the Boltzmann weight to be complex. This is the “complex action problem” or the “sign problem”. A conventional way to circumvent this problem is to calculate the partition function $\mathcal{Z}(\theta)$ by Fourier-transforming the topological charge distribution $P(Q)$, which is calculated with the real positive Boltzmann weight.^{3),4),5),6),7)} We call this the “Fourier transform method” (FTM).

*) E-mail: imachi@sci.kj.yamagata-u.ac.jp

***) E-mail: shinno@dirac.phys.saga-u.ac.jp

****) E-mail: yoneyama@cc.saga-u.ac.jp

Although this approach works well for small lattice volumes and/or in the strong coupling region, it does not work for large volumes and/or in the weak coupling region, due to flattening of the free energy density $f(\theta)$. This flattening phenomenon results from the error in $P(Q)$ obtained using Monte Carlo (MC) simulations and leads to a spurious phase transition for $\theta = \theta_f (< \pi)$. This is the sign problem. To overcome this problem requires exponentially increasing statistics.

As an alternative approach to the FTM,^{8),9)} we have applied the maximum entropy method (MEM) to the treatment of the sign problem. This method is based upon Bayes' theorem, and it has been widely used in various fields.^{10),11),12),13),14),15),16),17),18),19),20),21)} The MEM gives the most probable images by utilizing sets of data and our knowledge about these images. The probability distribution function, called the posterior probability, is given by the product of the likelihood function and the prior probability. The latter represents our knowledge about the image and the former indicates how data points are distributed around the true values. The prior probability is given as an entropy term, which plays the essential role to guarantee the uniqueness of the solution.

In order to investigate whether the MEM is applicable to the sign problem, we applied it to mock data, which were prepared by adding Gaussian noise to a model. In Ref. 21), a Gaussian $P(Q)$ was used. The corresponding free energy can be calculated analytically using the Poisson sum formula. As mock data, data with flattening and without flattening were prepared. We found that in both cases, the MEM reproduced smooth $f(\theta)$. The values of obtained $f(\theta)$ are in agreement with exact ones and the errors are reasonably small compared to those resulting when using the Fourier transform. These results might lead one to believe that the MEM has the effect of smoothing data and that, for this reason, it is not a suitable technique for detecting singular behaviors, such as phase transitions. To determine whether this is indeed the case, we analyzed some toy models that exhibit singular behavior originating from the characteristics of the models themselves.²²⁾ We found in Ref. 22) that in fact, the MEM can detect such singular behavior.

In the present paper, we apply the MEM to MC data of the CP^3 model. In order to check whether the MEM can treat real data in the θ term, data without flattening are used. Next, we investigate how the flattening phenomenon is observed within the MEM. In the MEM analysis, it is necessary to give prior information. Generally, an obtained image depends on this prior information. We systematically investigate the influence of this information on the most probable image. The uncertainty in the most probable image is estimated as an error. We also check the effectiveness of the MEM by considering this error.

This paper is organized as follows. In the following section, we summarize the formulations used in this work. Numerical results are presented in §3. In that section, we investigate in detail the behavior of the obtained most probable images. In the final section, conclusions and discussion are presented.

§2. Formulations

2.1. Topological charge distribution

The lattice action of the CP^{N-1} model with the θ term is defined by

$$S_\theta(\bar{z}, z) = S(\bar{z}, z) - i\theta Q(\bar{z}, z), \quad (2.1)$$

where S is a lattice action and Q is a topological charge. Complex scalar fields of the model are denoted by \bar{z} and z , where \bar{z} is the complex conjugate of z .

We choose an integer-valued topological charge,²³⁾

$$Q = \frac{1}{2\pi} \sum_{\square} A_{\square}, \quad (2.2)$$

where the plaquette contribution A_{\square} is given by

$$A_{\square} = \frac{1}{2} \sum_{\mu, \nu} \{A_{\mu}(n) + A_{\nu}(n + \hat{\mu}) - A_{\mu}(n + \nu) - A_{\nu}(n)\}. \pmod{2\pi} \quad (2.3)$$

Here we have $A_{\mu}(n) \equiv \arg[\bar{z}(n)z(n + \hat{\mu})]$, and these quantities satisfy $A_{\mu}(n) \in [-\pi, \pi]$.

As the conventional method for avoiding the complex Boltzmann weight, the partition function $\mathcal{Z}(\theta)$ is calculated by Fourier-transforming the topological charge distribution $P(Q)$:

$$\mathcal{Z}(\theta) = \sum_Q P(Q) e^{i\theta Q}. \quad (2.4)$$

The distribution $P(Q)$ is given by

$$P(Q) \equiv \frac{\int [d\bar{z}dz]_Q e^{-S(\bar{z}, z)}}{\int [d\bar{z}dz] e^{-S(\bar{z}, z)}}, \quad (2.5)$$

which is calculated with a real positive Boltzmann weight. The measure $[d\bar{z}dz]_Q$ expresses the meaning that the integral is restricted to configurations of \bar{z} and z with Q . Note that $P(Q)$ is normalized as $\sum_Q P(Q) = 1$.

We update configurations with the combined use of the overrelaxation and Metropolis algorithms. From the generated configurations, we measure Q and construct a histogram by counting the number of configurations with Q . Because the $P(Q)$ under consideration decreases rapidly as a function of Q , it is convenient to use the set method,²⁴⁾ in which an entire range of values of Q is divided into sets S_i ($i = 1, 2, 3, \dots$). In the present study, each of the sets S_i consists of 4 bins, $Q = 3i - 3, 3i - 2, 3i - 1$, and $3i$, and thus each set shares its two external bins with the adjacent sets. Explicitly, the shared bins are $Q = 3k$ ($k = 1, 2, 3, \dots$). In order to generate configurations more effectively and to reduce errors, the action is modified by adding a trial function $P_t(Q)$ satisfying

$$S_{eff} = S - \ln P_t(Q). \quad (2.6)$$

The form of $P_t(Q)$ is chosen as $P_t(Q) \propto e^{-\alpha Q^2}$ in the present study, where α is adjusted so that $P(Q)$ becomes almost flat in any given set, in order to reduce

errors. The power 2 of Q in $P_t(Q)$ is varied in a manner depending on the coupling constant.²⁵⁾

For the lattice action, we use a fixed point action (FP action)²⁶⁾ in order to reduce lattice artifacts. Because our simulations require a large number of measurements due to the θ term, we employ 9 coupling constants, which are limited to a short range and lie within one plaquette. With this action, it was shown in Ref. 25) that the lattice artifact is negligible up to somewhat small coupling constant, which corresponds to a correlation length of several units of the lattice spacing. We refer the reader to Ref. 25) for actual values of the coupling constants.

2.2. Flattening of the free energy density

The free energy density $f(\theta)$ is calculated by Fourier-transforming $P(Q)$ obtained by MC simulation. The quantity $f(\theta)$ is defined as

$$f(\theta) = -\frac{1}{V} \ln \sum_Q P(Q) e^{i\theta Q}, \quad (2.7)$$

where $V = L^2$, the square of the lattice size.

The MC data for $P(Q)$ consist of the true value, $\tilde{P}(Q)$, and its error, $\Delta P(Q)$. When the error at $Q = 0$ dominates because of the exponential damping of $P(Q)$, $f(\theta)$ is closely approximated by

$$f(\theta) \simeq -\frac{1}{V} \ln \left[e^{-V\tilde{f}(\theta)} + \Delta P(0) \right], \quad (2.8)$$

where $\tilde{f}(\theta)$ is the true value of $f(\theta)$. Because $\tilde{f}(\theta)$ is an increasing function of θ , as in the case of $\tilde{f}(\theta)$ derived from the Gaussian $P(Q)$ in the strong coupling region, $\Delta P(0)$ dominates for large values of θ . If $|\Delta P(0)| \simeq e^{-V\tilde{f}(\theta)}$ at $\theta = \theta_f$, then $f(\theta)$ becomes almost flat for $\theta \gtrsim \theta_f$. This is called ‘‘flattening of the free energy density’’, and it has been misleadingly identified as a first order phase transition, because the first derivative of $f(\theta)$ appears to jump at $\theta = \theta_f$. To avoid this problem, we must carry out a very large number of measurements in the FTM; indeed, the order of e^V measurements are needed.

2.3. MEM formalism

In this subsection, we briefly explain the MEM in terms of the θ term. (For details, see Ref. 21).)

In a parameter inference, such as the χ^2 fitting, the inverse Fourier transform

$$P(Q) = \int_{-\pi}^{\pi} \frac{d\theta}{2\pi} \mathcal{Z}(\theta) e^{-i\theta Q} \quad (2.9)$$

is used. In the numerical calculations, we use the discretized version of Eq. (2.9); $P(Q) = \sum_n K_{Q,n} \mathcal{Z}_n$, where $K_{Q,n}$ is the Fourier integral kernel and $\mathcal{Z}_n \equiv \mathcal{Z}(\theta_n)$. In order for the continuous function $\mathcal{Z}(\theta)$ to be reconstructed, a sufficient number of values of θ , which we denote by N_θ , is required so that the relation $N_\theta > N_Q$ holds, where N_Q represents the number of data points in $P(Q)$ ($Q = 0, 1, \dots, N_Q - 1$). A

straightforward application of the χ^2 fitting to the case $N_\theta > N_Q$ leads to degenerate solutions. This is an ill-posed problem.

The maximum entropy method is one promising tool to solve this ill-posed problem, and it gives a unique solution. The MEM is based upon Bayes' theorem, expressed as

$$\text{prob}(\mathcal{Z}(\theta)|P(Q), I) = \frac{\text{prob}(P(Q)|\mathcal{Z}(\theta), I) \text{prob}(\mathcal{Z}(\theta)|I)}{\text{prob}(P(Q)|I)}, \quad (2.10)$$

where $\text{prob}(A|B)$ is the conditional probability that A occurs under the condition that B occurs. The posterior probability $\text{prob}(\mathcal{Z}(\theta)|P(Q), I)$ is the probability that the partition function $\mathcal{Z}(\theta)$ is realized when the MC data $\{P(Q)\}$ and prior information I are given. The likelihood function $\text{prob}(P(Q)|\mathcal{Z}(\theta), I)$ is given by

$$\text{prob}(P(Q)|\mathcal{Z}(\theta), I) = \frac{1}{X_L} e^{-\frac{1}{2}\chi^2}, \quad (2.11)$$

where X_L is a normalization constant and χ^2 is a standard χ^2 function.

The probability $\text{prob}(\mathcal{Z}(\theta)|I)$, which guarantees the uniqueness of the solution, is given in terms of an entropy S as

$$\text{prob}(\mathcal{Z}(\theta)|I) = \frac{1}{X_S(\alpha)} e^{-\alpha S}, \quad (2.12)$$

where α and $X_S(\alpha)$ are a positive parameter and an α -dependent normalization constant, respectively. As S , the Shannon-Jaynes entropy is conventionally employed:

$$S = \sum_{n=1}^{N_\theta} \left[\mathcal{Z}_n - m_n - \mathcal{Z}_n \ln \frac{\mathcal{Z}_n}{m_n} \right]. \quad (2.13)$$

Here $m_n \equiv m(\theta_n)$ represents a default model.

The posterior probability $\text{prob}(\mathcal{Z}_n|P(Q), I)$, thus, is given by

$$\text{prob}(\mathcal{Z}_n|P(Q), I, \alpha, m) = \frac{1}{X_L X_S(\alpha)} e^{-\frac{1}{2}\chi^2 + \alpha S} \equiv \frac{e^{W[\mathcal{Z}]}}{X_L X_S(\alpha)}, \quad (2.14)$$

where it is explicitly expressed that α and m are regarded as new knowledge in $\text{prob}(\mathcal{Z}_n|P(Q), I, \alpha, m)$. For the prior information I , we impose the criterion

$$\mathcal{Z}_n > 0, \quad (2.15)$$

so that $\text{prob}(\mathcal{Z}_n \leq 0|I, \alpha, m) = 0$.

The most probable image of \mathcal{Z}_n , denoted as $\hat{\mathcal{Z}}_n$, is calculated according to the following procedures.^{12),21)}

1. Maximizing $W[\mathcal{Z}]$ to obtain the most probable image $\mathcal{Z}_n^{(\alpha)}$ for a given α :

$$\frac{\delta}{\delta \mathcal{Z}_n} W[\mathcal{Z}] |_{\mathcal{Z}=\mathcal{Z}^{(\alpha)}} = \frac{\delta}{\delta \mathcal{Z}_n} \left(-\frac{1}{2}\chi^2 + \alpha S \right) |_{\mathcal{Z}=\mathcal{Z}^{(\alpha)}} = 0. \quad (2.16)$$

2. Averaging $\mathcal{Z}_n^{(\alpha)}$ to obtain the α -independent most probable image $\hat{\mathcal{Z}}_n$:

$$\hat{\mathcal{Z}}_n = \int d\alpha \mathcal{Z}_n^{(\alpha)} \text{prob}(\alpha|P(Q), I, m). \quad (2.17)$$

The range of integration is determined so that the relation $\text{prob}(\alpha|P(Q), I, m) \geq \text{prob}(\hat{\alpha}|P(Q), I, m)/10$ holds, where $\text{prob}(\alpha|P(Q), I, m)$ is maximized at $\alpha = \hat{\alpha}$.

3. Error estimation:

The error of the most probable output image $\hat{\mathcal{Z}}_n$ is calculated as the uncertainty of the image, which takes into account the correlations of the images $\hat{\mathcal{Z}}_n$ among various values of θ_n :

$$\langle (\delta \hat{\mathcal{Z}}_n)^2 \rangle \equiv \int d\alpha \langle (\delta \mathcal{Z}_n^{(\alpha)})^2 \rangle \text{prob}(\alpha|P(Q), I, m). \quad (2.18)$$

Here $\delta \hat{\mathcal{Z}}_n$ and $\delta \mathcal{Z}_n^{(\alpha)}$ represent the error in $\hat{\mathcal{Z}}_n$ and that in $\mathcal{Z}_n^{(\alpha)}$, respectively.

2.4. The most probable image and the parameter α

In the MEM formalism, a real positive parameter α is introduced. This parameter plays the role of the trade-off between S and χ^2 . The most probable value of α is determined by the posterior probability of α , $\text{prob}(\alpha|P(Q), I, m)$, appearing in Eq. (2.17). The probability $\text{prob}(\alpha|P(Q), I, m)$ is given by

$$\text{prob}(\alpha|P(Q), I, m) \equiv P(\alpha) \propto g(\alpha) e^{W(\alpha) + \Lambda(\alpha)}, \quad (2.19)$$

where $W(\alpha) \equiv W[\mathcal{Z}^{(\alpha)}]$ and $2\Lambda(\alpha) \equiv \sum_k \ln\{\alpha/(\alpha + \lambda_k(\alpha))\}$. The function $\Lambda(\alpha)$ represents the contribution of fluctuations of $\mathcal{Z}(\theta)$ around $\mathcal{Z}^{(\alpha)}(\theta)$, and the quantities $\lambda_k(\alpha)$ are the eigenvalues of the real symmetric matrix

$$\Omega_{n,m} \equiv \frac{1}{2} \sqrt{\mathcal{Z}_m} \frac{\partial^2 \chi^2}{\partial \mathcal{Z}_m \partial \mathcal{Z}_n} \sqrt{\mathcal{Z}_n} |_{\mathcal{Z}=\mathcal{Z}^{(\alpha)}}. \quad (2.20)$$

Here, the function $g(\alpha)$ represents the prior probability of α and is chosen according to prior information. In general, two types of $g(\alpha)$ are employed, one according to Laplace's rule, $g_{\text{Lap}}(\alpha) = \text{const}$, and one according to Jeffrey's rule, $g_{\text{Jef}}(\alpha) = 1/\alpha$. The latter rule is determined by requiring that $P(\alpha)$ be invariant with respect to a change in scale, because α is a scale factor. The former rule means that we have no knowledge about the prior information of α . In general, the most probable image $\hat{\mathcal{Z}}(\theta)$ depends on $g(\alpha)$. In the present study, we investigate the sensitivity of $\hat{\mathcal{Z}}(\theta)$ to the choice of $g(\alpha)$. This is done by studying the quantity

$$\Delta(\theta) \equiv \frac{|\hat{\mathcal{Z}}_{\text{Lap}}(\theta) - \hat{\mathcal{Z}}_{\text{Jef}}(\theta)|}{(\hat{\mathcal{Z}}_{\text{Lap}}(\theta) + \hat{\mathcal{Z}}_{\text{Jef}}(\theta))/2}, \quad (2.21)$$

where $\hat{\mathcal{Z}}_{\text{Lap}}(\theta)$ and $\hat{\mathcal{Z}}_{\text{Jef}}(\theta)$ represent the most probable images according to Laplace's rule and Jeffrey's rule, respectively. The quantity $\Delta(\theta)$ is a relative difference, which is defined as the absolute value of the difference between $\hat{\mathcal{Z}}_{\text{Lap}}(\theta)$ and $\hat{\mathcal{Z}}_{\text{Jef}}(\theta)$ divided by the average of the two.

§3. Numerical results

3.1. Flattening in the Monte Carlo data

In this study, we carried out Monte Carlo simulations of the CP³ model with the fixed point action. We fixed the coupling constant β to 3.0 and the lattice size L to 38 and 50. The corresponding correlation length is approximately 7 in units of the lattice spacing. We employed the set method and the trial function method. The total number of measurements for each set was at least on the order of 10^6 . Parameter values used in the simulations are listed in Table I, where $Q_{\min} - Q_{\max}$ represents the range of the topological charge with which MC simulations were performed. It is noted that all data, except for $L = 38$ and 50, were obtained in a previous study.²⁵⁾

Table I. Parameter values used in the MC simulations of the CP³ model with the FP action. For the MEM analysis, new MC simulations were performed for $L = 38$ and 50.

β	L	$Q_{\min} - Q_{\max}$	total number of measurements (M/set)
3.0	12	0-30	10.0
	24	0-18	10.0
	32	0-24	3.0
	38	0-27	5.0
	46	0-33	1.0
	50	0-15	30.0
	56	0-18	5.0

Figure 1 displays the topological charge distribution $P(Q)$ (left panel) and the free energy density $f(\theta)$ (right panel) calculated by use of the FTM. The error in $f(\theta)$ was calculated using the jackknife method.

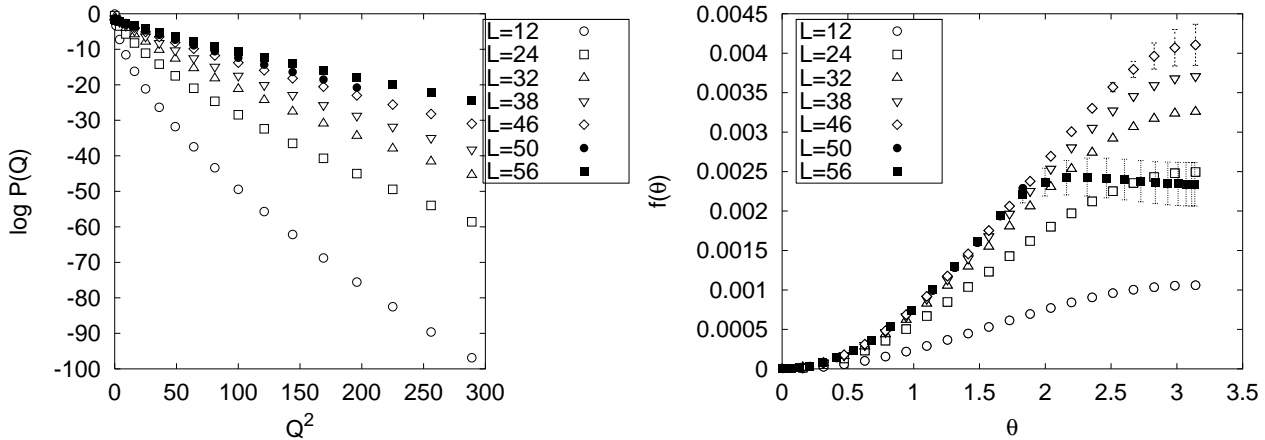


Fig. 1. Topological charge distributions $P(Q)$ (left panel) and free energy densities $f(\theta)$ (right panel) of the CP³ model for $\beta = 3.0$ and various lattice sizes L .

In the right panel of Fig. 1, it is observed that $f(\theta)$ depends on L . The free energy $f(\theta)$ increases as a function of L . For $\theta \lesssim 2.0$, $f(\theta)$ seems to approach an asymptotic line as the lattice volume increases ($L \geq 38$). For $\theta > 2.0$, by contrast,

the finite size effect in $f(\theta)$ is clearly observed. For $L = 56$, flattening is clearly seen. For $L = 50$, $f(\theta)$ is not plotted for $\theta \gtrsim 2.0$, because in this case negative values of $\mathcal{Z}(\theta)$ appear. We also call this behavior “flattening” for the same reason that the error in $P(Q)$ causes the FTM to become invalid (see §2.2). Although the total number of measurements carried out here is as large as 3×10^7 in each set for $L = 50$, flattening is still observed.

3.2. MEM analysis of the Monte Carlo data

As shown in the previous subsection, $f(\theta)$ exhibits flattening phenomena for $L = 50$ and 56 , while it behaves smoothly for smaller volumes in the FTM. In the present study, we systematically study flattening in terms of the MEM. For this purpose, the data for $L = 38$ and 50 are used.

In our analysis, three types of the default models are used: (i) $m_c(\theta) = \text{const}$; (ii) $m_G(\theta) = \exp[-\gamma \frac{\ln 10}{\pi^2} \theta^2]$; (iii) $m(\theta) = \hat{\mathcal{Z}}(\theta)$ for smaller volumes. In case (i), three values of $m_c(\theta)$, 1.0 , 1.0×10^{-3} and 1.0×10^{-5} , are employed, and only the results for $m_c(\theta) = 1.0$ are presented. Case (ii) is the Gaussian default model, and the parameter γ in $m_G(\theta)$ is varied over a wide range in the analysis. In case (iii), to analyze the data for the lattice size L_0 , images $\hat{\mathcal{Z}}(\theta)$ obtained from the MEM analysis for smaller volumes are used as default models. This is because we believe that $\mathcal{Z}(\theta)$ for smaller volumes might have properties similar to those for L_0 . Such $\hat{\mathcal{Z}}(\theta)$ may be regarded as prior information. For $L_0 = 50$, $\hat{\mathcal{Z}}(\theta)$ for $L = 24, 32$ and 38 are employed as the default models. These are denoted as $m_{L/L_0}(\theta) = m_{L/50}(\theta)$. Throughout this paper, it is understood, unless otherwise stated, that Laplace’s rule is used for $g(\alpha)$. The number N_Q is so chosen that $P(Q) \geq 10^{-18}$ holds for $L = 38$ and $P(Q) \geq 10^{-11}$ holds for $L = 50$. The function χ^2 in Eq. (2-11) is given in terms of the inverse covariance matrix of the MC data $\{P(Q)\}$. The inverse matrix is calculated with such precision that the product of the covariance matrix and its inverse has off-diagonal elements that are no larger than $\mathcal{O}(10^{-30})$. With these conditions, the value of N_Q is 5 for $L = 38$ and 7 for $L = 50$. It is noted that the analysis was performed with quadruple precision in order to properly reproduce $\hat{\mathcal{Z}}(\theta)$, which ranges over many orders.

3.2.1. Non-flattening case

Firstly, we apply the MEM to the data without flattening ($L = 38$). The left panel of Fig. 2 displays $\mathcal{Z}^{(\alpha)}(\theta)$ for a given α . Here, $m_c(\theta)$ and $m_G(\theta)$ with $\gamma = 1.0$ are used as the default models. The partition function obtained using the FTM, $\mathcal{Z}_{\text{Four}}(\theta)$, is also plotted for comparison. For each $m(\theta)$, the α dependence of $\mathcal{Z}^{(\alpha)}(\theta)$ is almost indiscernible for $\alpha \in [10, 100]$. It is seen that all the images have only very weak dependence on $m(\theta)$ over the entire range of values of θ . It is also observed that all the results of the MEM are consistent with those of the FTM. In the right panel, it is seen that $P(\alpha)$ depends on $m(\theta)$. The peaks of all the $P(\alpha)$ are located in the range $\alpha \leq 50$. The most probable image $\hat{\mathcal{Z}}(\theta)$ is calculated by using Eq. (2-17). The integrals over α are trivial, because $\mathcal{Z}^{(\alpha)}(\theta)$ depends on α only very weakly over the range of integration. Thus, it is expected that the values of $\hat{\mathcal{Z}}(\theta)$ for various $m(\theta)$ agree with those of $\mathcal{Z}_{\text{Four}}(\theta)$ over the entire range of values of θ . In fact, we

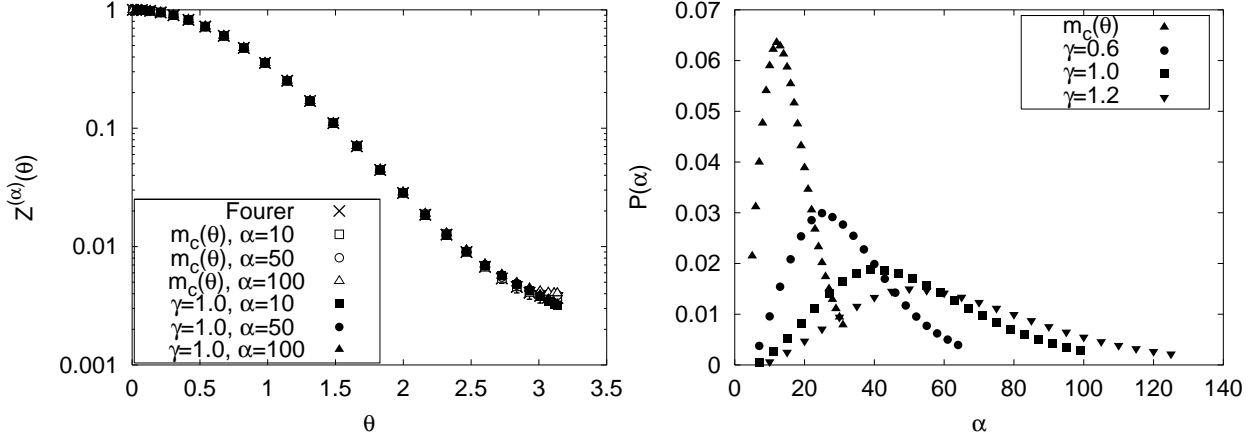


Fig. 2. Images $Z^{(\alpha)}(\theta)$ for a given α (left panel) and probabilities $P(\alpha)$ in the non-flattening case ($L = 38$). In the left panel, $m_c(\theta)$ and $m_G(\theta)$ with $\gamma = 1.0$ are used. In addition, $m_G(\theta)$ with $\gamma = 0.6$ and 1.2 are used in the right panel.

find that all the $\hat{Z}(\theta)$ are equal to $Z_{\text{Four}}(\theta)$ within numerical errors. The errors are calculated according to the procedure 3 outlined in §2.3. Some of these results are listed in Table II, specifically, the values of $\hat{Z}(\theta)$ for various $m_G(\theta)$ and $Z_{\text{Four}}(\theta)$ at three values of θ . These values of θ are chosen as representatives; the first value is $\theta = 2.00$. Up to this value, the asymptotic line of $f(\theta)$ is observed (see Fig. 1). The second one is $\theta = 3.14$ chosen as a value near π . The third one is $\theta = 2.60$, chosen as a value approximately halfway between these two. It is noted that the errors in $\hat{Z}(\theta)$ are rather small for the entire range of values of θ .

Table II. Values of the most probable images $\hat{Z}(\theta)$ at $\theta = 2.00$, 2.60 and 3.14 . As default models, $m_G(\theta)$ with $\gamma = 0.6$, 1.0 and 1.2 were used. For comparison, $Z_{\text{Four}}(\theta)$ is also listed.

θ	$Z_{\text{Four}}(\theta)$	$\hat{Z}_{\gamma=0.6}(\theta)$	$\hat{Z}_{\gamma=1.0}(\theta)$	$\hat{Z}_{\gamma=1.2}(\theta)$
2.00	$2.840(46) \times 10^{-2}$	$2.846(100) \times 10^{-2}$	$2.844(81) \times 10^{-2}$	$2.844(73) \times 10^{-2}$
2.60	$0.675(47) \times 10^{-2}$	$0.696(57) \times 10^{-2}$	$0.707(46) \times 10^{-2}$	$0.712(41) \times 10^{-2}$
3.14	$0.367(51) \times 10^{-2}$	$0.343(52) \times 10^{-2}$	$0.322(42) \times 10^{-2}$	$0.312(37) \times 10^{-2}$

The calculations discussed above were performed using Eq. (2·17) with Laplace's rule. When Jeffrey's rule is employed, the peak of $P(\alpha)$ appears at a value of α smaller than that in the case of Laplace's rule. The probability $P_{\text{Lap}}(\alpha)$ for $\gamma = 1.2$, for example, peaks at $\alpha = 50$, while $P_{\text{Jef}}(\alpha)$ peaks at $\alpha = 35$. (Here, $P_{\text{Lap}}(\alpha)$ and $P_{\text{Jef}}(\alpha)$ represent $P(\alpha)$ for Laplace's and Jeffrey's rules, respectively.) Although $P_{\text{Lap}}(\alpha)$ and $P_{\text{Jef}}(\alpha)$ peak at different values of α , similar images for $\hat{Z}(\theta)$ are obtained with slightly different errors, because $Z^{(\alpha)}(\theta)$ is almost independent of α [see Eq. (2·17)]. We, thus, find in the non-flattening case that the MEM gives most probable images that are almost independent of the prior information and is consistent with the FTM.

3.2.2. Flattening case

Now that we have found that the MEM is applicable to the analysis of the MC data, let us turn to the analysis of data with flattening ($L = 50$). In Fig. 3, we show $\mathcal{Z}_{\text{Four}}(\theta)$ obtained using the FTM for data with 30.0M/set. Although $\mathcal{Z}_{\text{Four}}(\theta)$ behaves smoothly, its errors are large over a large range of values of θ (specifically for $\theta \gtrsim 2.4$). These large errors result from the error propagation of $P(Q)$ through the Fourier transform. Let us here consider its effect by studying a quantity which represents the error propagation of $P(Q)$ in the case that there is no correlation of the distribution $P(Q)$ for different values of Q ,

$$\epsilon \equiv \sum_Q |\Delta P(Q)|. \quad (3-1)$$

Here, $\epsilon = 3.610 \times 10^{-4}$, and the value of $\mathcal{Z}_{\text{Four}}(\theta)$ is comparable with that of ϵ at $\theta \simeq 2.4$. Figure 3 displays that when the value of $\mathcal{Z}_{\text{Four}}(\theta)$ is smaller than that of ϵ , the error in $\mathcal{Z}_{\text{Four}}(\theta)$ becomes large. This approximately holds for all cases we have investigated. In the MEM, ϵ could be an indicator for the influence of the error of $P(Q)$ on $\hat{\mathcal{Z}}(\theta)$. This point is discussed in the following. In the analysis of data with flattening, much care is required.²¹⁾

In order to properly evaluate $\hat{\mathcal{Z}}(\theta)$ obtained using the MEM, we carefully investigate (i) the statistical fluctuations of $\hat{\mathcal{Z}}(\theta)$, (ii) the $g(\alpha)$ dependence of $\hat{\mathcal{Z}}(\theta)$, and (iii) the relative error in $\hat{\mathcal{Z}}(\theta)$.

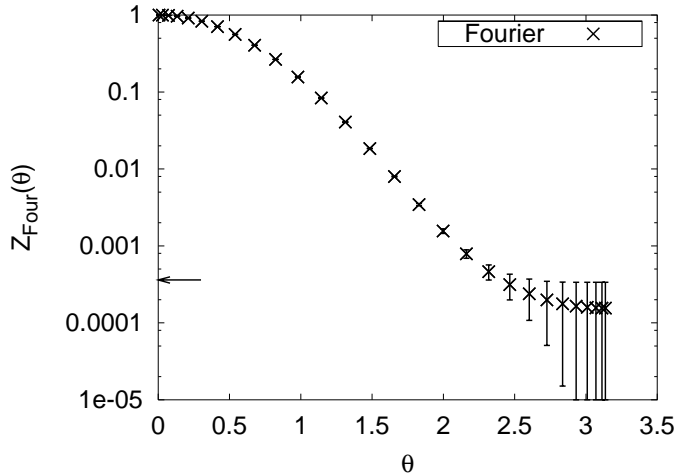


Fig. 3. Partition function $\mathcal{Z}_{\text{Four}}(\theta)$ obtained using the FTM. The number of measurements is 30.0M/set. The arrow indicates the value of ϵ ($= 3.610 \times 10^{-4}$). The errors were calculated with the jackknife method.

(i) The statistical fluctuations of $\hat{\mathcal{Z}}(\theta)$

Figure 4 displays five images $\hat{\mathcal{Z}}(\theta)$, which are called Data A, B, C, D and E, respectively. These images were calculated from the data with 2.0M/set, which are independent of each other. The uncertainties in $\hat{\mathcal{Z}}(\theta)$ calculated with Eq. (2-18) are indicated as errors in Fig. 4. As a default model, the Gaussian default with $\gamma = 5.0$

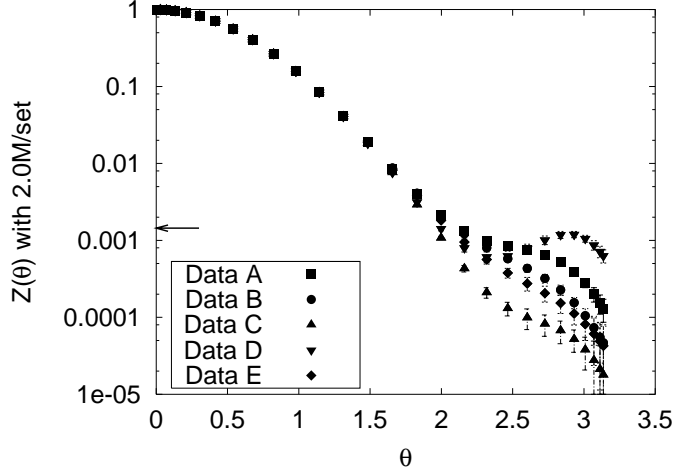


Fig. 4. The five most probable images $\hat{Z}(\theta)$ for $L = 50$ with 2.0M/set. Here, the Gaussian default model with $\gamma = 5.0$ was used. The arrow indicates the value of ϵ ($= 1.441 \times 10^{-3}$) in Data A. The errors in $\hat{Z}(\theta)$ were calculated by use of Eq. (2-18).

were used. It is seen that all the images $\hat{Z}(\theta)$ fall on the same curve for $\theta \lesssim 2.0$, while they behave differently for $\theta \gtrsim 2.0$. The value of ϵ is at least 1.3×10^{-3} for these five sets of data, and the values of all the images $\hat{Z}(\theta)$ are smaller than that of ϵ for $\theta \gtrsim 2.0$. Figure 4 indicates that $\hat{Z}(\theta)$ fluctuates greatly when the value of $\hat{Z}(\theta)$ is smaller than that of ϵ .

To see how $\hat{Z}(\theta)$ depends on the statistics, we varied the number of measurements. We fixed the value of θ and chose the values $\theta = 2.31$ and 3.14 . The value $\theta = 2.31$ was chosen for the previously stated reason that $Z_{\text{Four}}(\theta)$ starts to contain large errors at this value for the data with 30.0M/set (see Fig. 3). Figure 5 displays

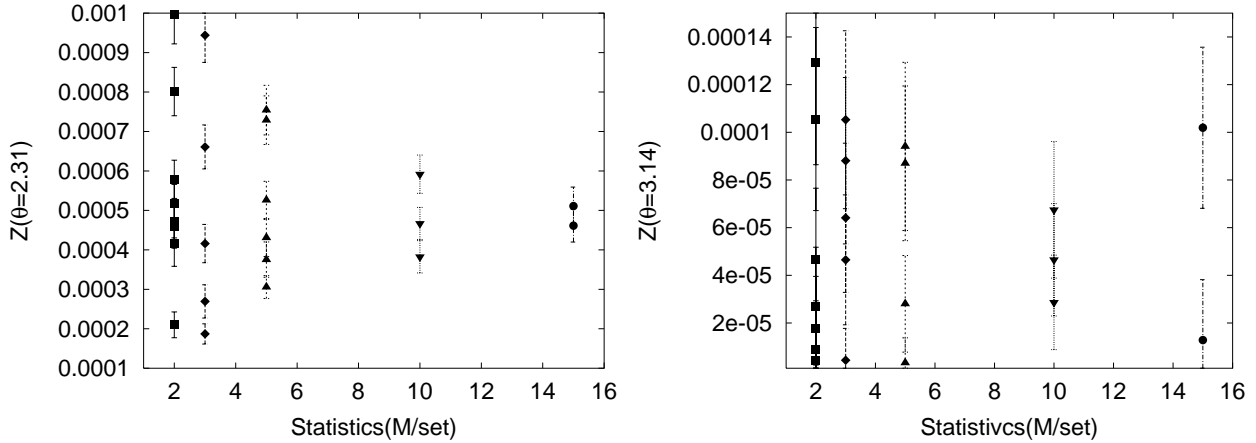


Fig. 5. Values of $\hat{Z}(\theta)$ for $\theta = 2.31$ (left panel) and 3.14 (right panel). The horizontal axis represents the number of measurements. Here, the Gaussian default model with $\gamma = 5.0$ was used.

$\hat{\mathcal{Z}}(\theta)$ for $\theta = 2.31$ (left panel) and 3.14 (right panel). The horizontal axis represents the number of measurements. In the left panel, it is seen that the fluctuations of $\hat{\mathcal{Z}}(2.31)$ become smaller as the number of measurements increases. In the right panel, it is seen that $\hat{\mathcal{Z}}(\theta)$ for 15.0M/set fluctuates as greatly as $\hat{\mathcal{Z}}(\theta)$ for 2.0M/set. In Table III, the values of $\hat{\mathcal{Z}}(\theta)$ for $\theta = 2.31, 2.60$ and 3.14 are listed for the cases of 20.0M/set, 26.0M/set and 30.0M/set. For $\theta = 2.31$ and 2.60, the images $\hat{\mathcal{Z}}(\theta)$ do not vary within the errors as the number of measurements increases. For $\theta = 3.14$, the value of $\hat{\mathcal{Z}}(\theta)$ varies significantly as the number of measurements increases. In the cases $\theta = 2.31$ and 2.60, the values of $\hat{\mathcal{Z}}(\theta)$ are comparable with that of ϵ for 30.0M/set ($\epsilon = 3.610 \times 10^{-4}$), while in the case $\theta = 3.14$, the value of $\hat{\mathcal{Z}}(\theta)$ is one order smaller than ϵ . This indicates that when the value of $\hat{\mathcal{Z}}(\theta)$ is smaller than that of ϵ , $\hat{\mathcal{Z}}(\theta)$ is strongly affected by the error in $P(Q)$. Hereafter, we concentrate on the data with 30.0M/set.

Table III. Values of $\hat{\mathcal{Z}}(\theta)$ for $\theta = 2.31, 2.60$ and 3.14. Here, the same default model as in Fig. 5 is used.

statistics(M/set)	$\hat{\mathcal{Z}}_{\gamma=5.0}(2.31)$	$\hat{\mathcal{Z}}_{\gamma=5.0}(2.60)$	$\hat{\mathcal{Z}}_{\gamma=5.0}(3.14)$
20.0	$4.07(39) \times 10^{-4}$	$2.30(31) \times 10^{-4}$	$3.93(22) \times 10^{-5}$
26.0	$4.22(40) \times 10^{-4}$	$2.69(33) \times 10^{-4}$	$5.83(26) \times 10^{-5}$
30.0	$4.58(40) \times 10^{-4}$	$2.81(33) \times 10^{-4}$	$5.37(26) \times 10^{-5}$

(ii) The $g(\alpha)$ dependence of $\hat{\mathcal{Z}}(\theta)$

The most probable image $\hat{\mathcal{Z}}(\theta)$ is obtained by performing the integral with respect to α according to the procedure 2 outlined in §2.3. The probability $P(\alpha)$ in Eq. (2.19) involves the prior probability of α , $g(\alpha)$. In the present study, we investigate the $g(\alpha)$ dependence of $\hat{\mathcal{Z}}(\theta)$ by calculating Eq. (2.21).

Before calculating $\Delta(\theta)$, we investigate how $g(\alpha)$ affects the behavior of $P(\alpha)$. From the definition given in §2.4, the following relation holds, up to the normalization constant between $P_{\text{Lap}}(\alpha)$ and $P_{\text{Jef}}(\alpha)$:

$$P_{\text{Jef}}(\alpha) \propto g_{\text{Jef}}(\alpha) P_{\text{Lap}}(\alpha) = \frac{1}{\alpha} P_{\text{Lap}}(\alpha). \quad (3.2)$$

The probability $g_{\text{Jef}}(\alpha)$ deforms the shape of $P_{\text{Lap}}(\alpha)$ and shifts the location of its peak.¹³⁾ It was shown in Ref. 12) that when $P_{\text{Lap}}(\alpha)$ is concentrated around its maximum at $\alpha = \hat{\alpha}$, the peaks of $P_{\text{Lap}}(\alpha)$ and $P_{\text{Jef}}(\alpha)$ are located at nearly equal values of α , and $\hat{\mathcal{Z}}(\theta)$ is insensitive to the choice of $g(\alpha)$. We quantitatively determine the amount by which $g_{\text{Jef}}(\alpha)$ shifts the location of the peak of $P_{\text{Lap}}(\alpha)$ in the following.

The derivative of $P(\alpha)$ with respect to α ,

$$\frac{dP(\alpha)}{d\alpha} = \left[\frac{1}{2\alpha} \sum_k \frac{\lambda_k(\alpha)}{\alpha + \lambda_k(\alpha)} + S(\alpha) + \frac{d \ln g(\alpha)}{d\alpha} - \frac{1}{2} \frac{d\chi^2(\alpha)}{d\alpha} + \alpha \frac{dS(\alpha)}{d\alpha} - \frac{1}{2} \sum_k \frac{1}{\alpha + \lambda_k(\alpha)} \frac{d\lambda_k(\alpha)}{d\alpha} \right] P(\alpha), \quad (3.3)$$

is vanishing at $\alpha = \hat{\alpha}$. It is noted that $\chi^2(\alpha)$, $S(\alpha)$ and $\{\lambda_k(\alpha)\}$ depend implicitly on α through $\mathcal{Z}^{(\alpha)}(\theta)$, calculated using Eq. (2.16). We obtain

$$\hat{\alpha}_{\text{Lap}} S(\hat{\alpha}_{\text{Lap}}) = -\frac{1}{2}N_g + [\text{derivative terms}], \quad (\text{Laplace's rule}) \quad (3.4)$$

$$\hat{\alpha}_{\text{Jef}} S(\hat{\alpha}_{\text{Jef}}) = -\frac{1}{2}(N_g - 2) + [\text{derivative terms}], \quad (\text{Jeffrey's rule}) \quad (3.5)$$

where “derivative terms” represents the derivatives of $\chi^2(\alpha)$, $S(\alpha)$ and $\lambda_k(\alpha)$, and $\hat{\alpha}_{\text{Lap}}$ and $\hat{\alpha}_{\text{Jef}}$ denote $\hat{\alpha}$ for Laplace’s and Jeffrey’s rules, respectively. Here, $N_g \equiv \sum_k \lambda_k(\hat{\alpha})/(\hat{\alpha} + \lambda_k(\hat{\alpha}))$, and N_g represents the number of effectively independent measurements, because the value of the $\lambda_k(\hat{\alpha})$ contributes approximately 1 to the summation when $\lambda_k(\hat{\alpha}) \gg \hat{\alpha}$. Note that since the quantities $\lambda_k(\alpha)$ are independent of the choice of $g(\alpha)$, N_g is also insensitive to $g(\alpha)$. For simplicity, let us ignore these “derivative terms” for the time being. With the relative difference between the two values of $\hat{\alpha}$,

$$r_{\hat{\alpha}} \equiv \frac{\hat{\alpha}_{\text{Lap}} - \hat{\alpha}_{\text{Jef}}}{\hat{\alpha}_{\text{Lap}}}, \quad (3.6)$$

we obtain, from Eqs. (3.4) and (3.5),

$$r_{\hat{\alpha}} = \frac{2}{N_g}, \quad (3.7)$$

because the derivative of $S(\alpha)$ is vanishing and $S(\hat{\alpha}_{\text{Lap}}) \simeq S(\hat{\alpha}_{\text{Jef}})$. Hence, the relative difference between the values of $\hat{\alpha}$, $r_{\hat{\alpha}}$, to good approximation depends only on N_g . When N_g is larger than 2, $r_{\hat{\alpha}}$ is negligible, and the peaks of $P_{\text{Lap}}(\alpha)$ and $P_{\text{Jef}}(\alpha)$ could be located at almost equal values of α . In case that the “derivative terms” cannot be ignored, however, using only N_g , one cannot properly estimate to what extent the location of the peak moves. In such a case, we need to resort to numerical calculations.

Let us investigate the behavior of $P(\alpha)$ in our data; specifically, we check whether the derivatives of $\chi^2(\alpha)$, $S(\alpha)$ and $\{\lambda_k(\alpha)\}$ are negligible and determine the distance between the peaks of $P_{\text{Lap}}(\alpha)$ and $P_{\text{Jef}}(\alpha)$. The values of $\hat{\alpha}$, $\hat{\alpha}S(\hat{\alpha})$, $N_g/2$ and $|\hat{\alpha}S(\hat{\alpha}) + N_g/2| \equiv D$ for various $m_G(\theta)$ are listed in Table IV in the case of Laplace’s rule. As shown in Eq. (3.4), the value of D provides a criterion for determining whether or not the “derivative terms” can be ignored.

Firstly, we focus on the $\gamma = 5.0$ case. In Eq. (3.4), D makes a smaller contribution to $\hat{\alpha}_{\text{Lap}} S(\hat{\alpha}_{\text{Lap}})$ than does $N_g/2$ ($D \simeq 0.04 \times N_g/2$), and hence the “derivative terms” can be ignored. It is thus expected that Eq. (3.7) holds. Substituting $\hat{\alpha}_{\text{Lap}}$ and N_g in Table IV into Eq. (3.7), we obtain $\hat{\alpha}_{\text{Jef}} \simeq 287$. With Jeffrey’s rule, on the other hand, $P_{\text{Jef}}(\alpha)$ gives $\hat{\alpha}_{\text{Jef}} = 293$. We thus find good agreement between the values of $\hat{\alpha}_{\text{Jef}}$ obtained in these two ways. Next, we determine the distance between the peaks of $P_{\text{Lap}}(\alpha)$ and $P_{\text{Jef}}(\alpha)$. Because the value of N_g is comparable to 2 ($r_{\hat{\alpha}} \simeq 0.27$), it is expected that the peaks of $P_{\text{Lap}}(\alpha)$ and $P_{\text{Jef}}(\alpha)$ could appear at somewhat separated values of α . It is shown that this is indeed the case in the left panel of Fig. 6.

Now let us consider the other cases of the default model $m_G(\theta)$ in Table IV. The values of D are larger than that for $\gamma = 5.0$: we have $D \simeq 0.67 \times N_g/2$, $D \simeq 0.18 \times N_g/2$ and $D \simeq 0.30 \times N_g/2$ for $\gamma = 8.0, 10.0$ and 13.0 , respectively. In these cases, the “derivative terms” are not negligible, and Eq. (3.7) no longer holds. The probabilities $P(\alpha)$ for Laplace’s and Jeffrey’s rules give $r_{\hat{\alpha}} \simeq 0.20, 0.14$ and 0.13 for $\gamma = 8.0, 10.0$ and 13.0 , respectively. The right panel of Fig. 6 displays both $P_{\text{Lap}}(\alpha)$ and $P_{\text{Jef}}(\alpha)$ for $\gamma = 13.0$. In this figure, the peaks of $P_{\text{Lap}}(\alpha)$ and $P_{\text{Jef}}(\alpha)$ are seen to be located at different values of α . Similar behavior of $P(\alpha)$ is obtained for the other default models $m(\theta)$.

Table IV. Values of $\hat{\alpha}_{\text{Lap}}$, $\hat{\alpha}_{\text{Lap}}S(\hat{\alpha}_{\text{Lap}})$, $-N_g/2$ and $D(\equiv |\hat{\alpha}_{\text{Lap}}S(\hat{\alpha}_{\text{Lap}}) + N_g/2|)$ for various $m_G(\theta)$ with Laplace’s rule. Here, $N_Q = 7$.

γ (Gaussian default)	$\hat{\alpha}_{\text{Lap}}$	$\hat{\alpha}_{\text{Lap}}S(\hat{\alpha}_{\text{Lap}})$	$-N_g/2$	$ \hat{\alpha}_{\text{Lap}}S(\hat{\alpha}_{\text{Lap}}) + N_g/2 \equiv D$
5.0	401	-3.358	-3.498	0.140($\simeq 0.04 \times N_g/2$)
8.0	10200	-0.992	-3.046	2.054($\simeq 0.67 \times N_g/2$)
10.0	1400	-2.653	-3.232	0.579($\simeq 0.18 \times N_g/2$)
13.0	460	-4.419	-3.410	1.009($\simeq 0.30 \times N_g/2$)

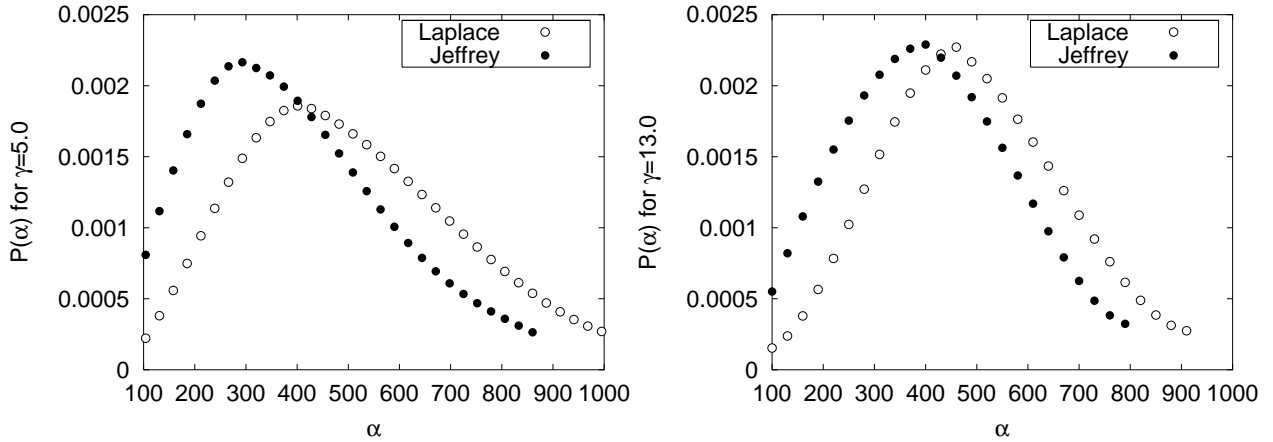


Fig. 6. $P_{\text{Lap}}(\alpha)$ and $P_{\text{Jef}}(\alpha)$. As the default models, Gaussian functions with $\gamma = 5.0$ (left panel) and 13.0 (right panel) were used.

Let us now study $\hat{\mathcal{Z}}(\theta)$. The α -dependent image $\mathcal{Z}^{(\alpha)}(\theta)$ affects the behavior of $\hat{\mathcal{Z}}(\theta)$ through the integral in Eq. (2.17):

$$\hat{\mathcal{Z}}(\theta) = \begin{cases} \int d\alpha P_{\text{Lap}}(\alpha)\mathcal{Z}^{(\alpha)}(\theta), & \text{(Laplace's rule)} \\ \int d\alpha P_{\text{Jef}}(\alpha)\mathcal{Z}^{(\alpha)}(\theta). & \text{(Jeffrey's rule)} \end{cases} \quad (3.8)$$

If $\mathcal{Z}^{(\alpha)}(\theta)$ does not vary over the range of integration in Eq. (3.8), $\mathcal{Z}^{(\alpha)}(\theta)$ can be factored out from the integral and we have $\hat{\mathcal{Z}}_{\text{Lap}}(\theta) = \hat{\mathcal{Z}}_{\text{Jef}}(\theta)$, due to the normalization of $P(\alpha)$. This is indeed the case for $\gamma = 5.0$: for $\theta = 2.60$, for example, the values of $\mathcal{Z}^{(\alpha)}(\theta)$ are 2.831×10^{-4} for $\alpha = 50$ and 2.797×10^{-4} for $\alpha = 1050$. The latter value of α is the upper limit of α , α_{max} , and the former one is the lower

limit of α , α_{\min} , in the integral. For the other default models listed in Table IV, by contrast, all the $\mathcal{Z}^{(\alpha)}(\theta)$ vary over several orders for $\theta \gtrsim 2.6$. For $\gamma = 13.0$, for example, the values of $\mathcal{Z}^{(\alpha)}(2.60)$ are 2.80×10^{-4} and 9.55×10^{-7} for $\alpha = \alpha_{\min} = 100$ and $\alpha = \alpha_{\max} = 910$, respectively. From these results, it is conjectured that $\hat{\mathcal{Z}}(\theta)$ is almost independent of $g(\alpha)$ for $\gamma = 5.0$ and depends strongly on $g(\alpha)$ for the other values of γ . In fact, no $g(\alpha)$ dependence is seen over the entire the range of values of θ for $\gamma = 5.0$, as shown in the left panel of Fig. 7, while in the right panel (depicting the situation for $\gamma = 13.0$), differences between these two are observed for $\theta \gtrsim 2.6$. Note that for $\theta \lesssim 2.0$, $\hat{\mathcal{Z}}_{\text{Lap}}(\theta)$ and $\hat{\mathcal{Z}}_{\text{Jef}}(\theta)$ fall on the same curve in both the $\gamma = 5.0$ and 13.0 cases.

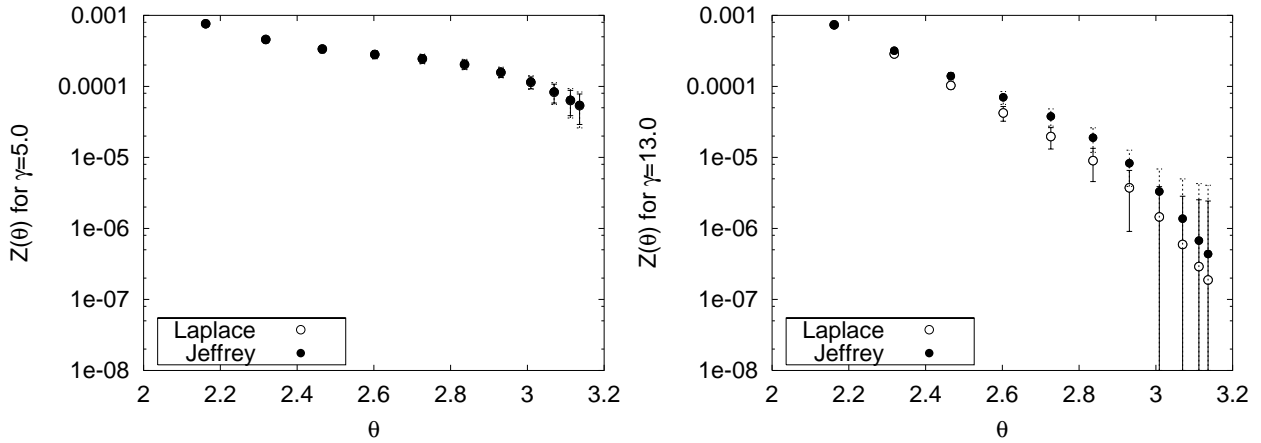


Fig. 7. $\hat{\mathcal{Z}}_{\text{Lap}}(\theta)$ and $\hat{\mathcal{Z}}_{\text{Jef}}(\theta)$ for $\theta \in [2.0, \pi]$. The default models used here are the same as in Fig. 6. The errors in $\hat{\mathcal{Z}}(\theta)$ were calculated using Eq. (2·18).

In order to estimate the influence of $g(\alpha)$ on $\hat{\mathcal{Z}}(\theta)$, we calculate $\Delta(\theta)$ given by Eq. (2·21). For a systematic estimation, the parameter γ in $m_G(\theta)$ is varied from 3.0 to 13.0. Figure 8 displays the values of $\Delta(\theta)$ at $\theta = 2.60$. The horizontal axis represents the value of γ . It is found that the value of $\Delta(\theta)$ is smallest for $\gamma = 5.0$ and becomes larger as the value of γ deviates from 5.0. Table V lists the values of $\Delta(\theta)$ for eight images among these with $\theta = 2.31, 2.60, 2.83$ and 3.14. In the case of $\gamma = 5.0$, the value of $\Delta(\theta)$ increases with θ for $\theta \gtrsim 2.6$. This behavior is also observed for the other $m(\theta)$. It is found that the values of $\Delta(\theta)$ for $\gamma = 3.0, 4.0, 5.0, m_{24/50}(\theta), m_{32/50}(\theta)$ and $m_{38/50}(\theta)$ are quite small over the entire range of values of θ and that the images $\mathcal{Z}^{(\alpha)}(\theta)$ for these six depend only very weakly on α over the range of integration in Eq. (2·17).

We now give a brief comment on ϵ in Eq. (3·1). The difference between $\hat{\mathcal{Z}}_{\text{Lap}}(\theta)$ and $\hat{\mathcal{Z}}_{\text{Jef}}(\theta)$ becomes significant at the value $\theta = \theta_\epsilon$, where $\hat{\mathcal{Z}}(\theta_\epsilon) \simeq \epsilon$ is satisfied, and $\Delta(\theta_\epsilon) \simeq 0.1$ holds; e.g., for $\gamma = 13.0$, we have $\theta_\epsilon \simeq 2.3$ (see Fig. 7). This is true for all cases in which $\gamma \geq 7.0$.

(iii) The relative error of $\hat{\mathcal{Z}}(\theta)$

Now that the $g(\alpha)$ dependence of $\hat{\mathcal{Z}}(\theta)$ has been systematically investigated, we next consider the uncertainty in $\hat{\mathcal{Z}}(\theta)$.

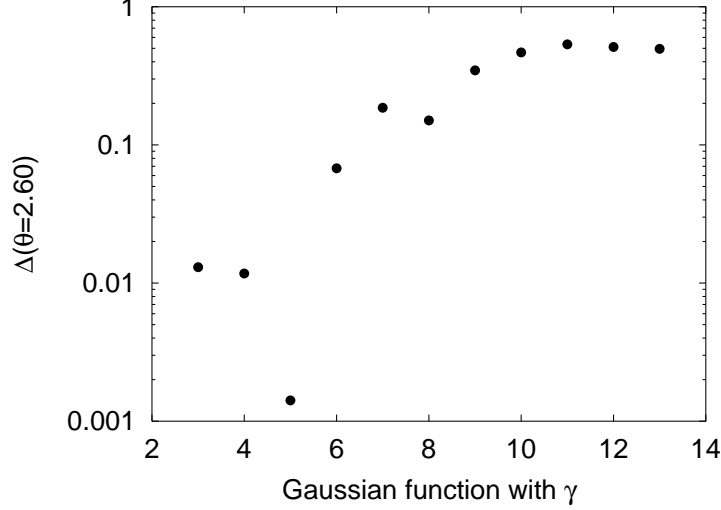


Fig. 8. Values of $\Delta(\theta)$ for $\theta = 2.60$. The Gaussian functions are used as the default models. The horizontal axis represents the value of γ in $m_G(\theta)$.

Table V. Values of $\Delta(\theta)$ at $\theta = 2.31, 2.60, 2.83$ and 3.14 for various $m(\theta)$.

default model	$\Delta(2.31)$	$\Delta(2.60)$	$\Delta(2.83)$	$\Delta(3.14)$
$m_G(\theta)$ with $\gamma = 3.0$	6.30×10^{-3}	1.30×10^{-2}	1.87×10^{-2}	2.24×10^{-2}
$m_G(\theta)$ with $\gamma = 5.0$	5.35×10^{-3}	1.41×10^{-3}	1.12×10^{-2}	1.84×10^{-2}
$m_G(\theta)$ with $\gamma = 8.0$	1.03×10^{-1}	1.50×10^{-1}	1.70×10^{-1}	1.75×10^{-1}
$m_G(\theta)$ with $\gamma = 10.0$	1.01×10^{-1}	4.67×10^{-1}	8.21×10^{-1}	9.60×10^{-1}
$m_G(\theta)$ with $\gamma = 13.0$	1.05×10^{-1}	4.96×10^{-1}	7.12×10^{-1}	7.95×10^{-1}
$m_{24/50}(\theta)$	3.44×10^{-3}	7.67×10^{-3}	1.13×10^{-2}	1.36×10^{-2}
$m_{32/50}(\theta)$	7.30×10^{-3}	1.57×10^{-2}	2.29×10^{-2}	2.72×10^{-2}
$m_{38/50}(\theta)$	1.30×10^{-2}	2.60×10^{-2}	3.65×10^{-2}	4.26×10^{-2}

Table VI. Values of $|\delta \hat{\mathcal{Z}}|/\hat{\mathcal{Z}}(\theta) \equiv |\delta \hat{\mathcal{Z}}(\theta)|/\hat{\mathcal{Z}}(\theta)$ for $\theta = 2.31, 2.60, 2.83$ and 3.14 . Here, the same default models as in Table V were used.

default model	$ \delta \hat{\mathcal{Z}} /\hat{\mathcal{Z}}(2.31)$	$ \delta \hat{\mathcal{Z}} /\hat{\mathcal{Z}}(2.60)$	$ \delta \hat{\mathcal{Z}} /\hat{\mathcal{Z}}(2.83)$	$ \delta \hat{\mathcal{Z}} /\hat{\mathcal{Z}}(3.14)$
$m_G(\theta)$ with $\gamma = 3.0$	1.57×10^{-1}	2.31×10^{-1}	2.91×10^{-1}	6.24×10^{-1}
$m_G(\theta)$ with $\gamma = 5.0$	8.82×10^{-2}	1.17×10^{-1}	1.44×10^{-1}	4.58×10^{-1}
$m_G(\theta)$ with $\gamma = 8.0$	2.21×10^{-2}	2.15×10^{-1}	1.93	56.84
$m_G(\theta)$ with $\gamma = 10.0$	3.48×10^{-2}	3.88×10^{-1}	1.86	40.69
$m_G(\theta)$ with $\gamma = 13.0$	6.88×10^{-2}	2.35×10^{-1}	4.93×10^{-1}	11.94
$m_{24/50}(\theta)$	2.70×10^{-1}	4.82×10^{-1}	6.54×10^{-1}	8.31×10^{-1}
$m_{32/50}(\theta)$	1.67×10^{-1}	2.73×10^{-1}	3.76×10^{-1}	4.82×10^{-1}
$m_{38/50}(\theta)$	1.03×10^{-1}	1.57×10^{-1}	2.12×10^{-1}	2.68×10^{-1}

The relative errors in $\hat{\mathcal{Z}}(\theta)$, $|\delta \hat{\mathcal{Z}}(\theta)|/\hat{\mathcal{Z}}(\theta)$, are displayed in Fig. 9, where $\delta \hat{\mathcal{Z}}(\theta)$ is calculated using Eq. (2-18). For comparison, $|\delta \mathcal{Z}_{\text{Four}}(\theta)|/\mathcal{Z}_{\text{Four}}(\theta)$ is also plotted. It is observed that all the relative errors increase with θ . In particular, those for $\gamma = 8.0, 10.0$ and 13.0 diverge for large θ ($\theta \gtrsim 2.6$). The value of $|\delta \hat{\mathcal{Z}}(\theta)|/\hat{\mathcal{Z}}(\theta)$ for $m_{24/50}(\theta)$ is comparable with that of $|\delta \mathcal{Z}_{\text{Four}}(\theta)|/\mathcal{Z}_{\text{Four}}(\theta)$, and those for the others

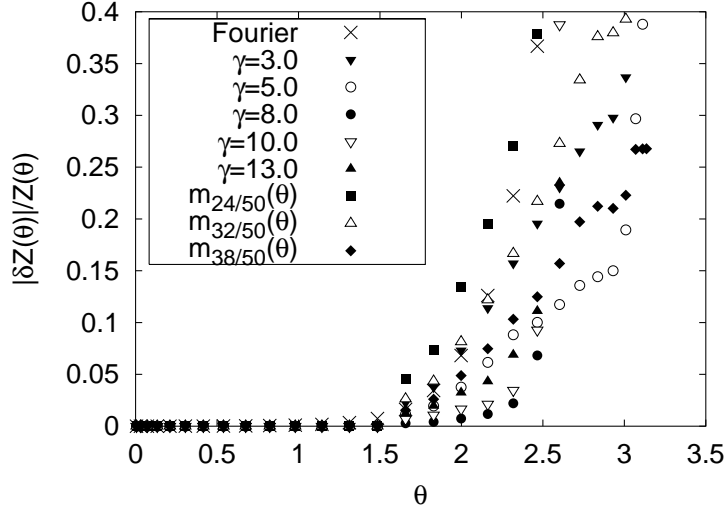


Fig. 9. Values of $|\delta\hat{\mathcal{Z}}(\theta)|/\hat{\mathcal{Z}}(\theta)$ for the selected default models. The results obtained with the Fourier method are also plotted.

are smaller than that of $|\delta\mathcal{Z}_{\text{Four}}(\theta)|/\mathcal{Z}_{\text{Four}}(\theta)$. To see in detail how $|\delta\hat{\mathcal{Z}}(\theta)|/\hat{\mathcal{Z}}(\theta)$ varies in the large θ region, we list $|\delta\hat{\mathcal{Z}}(\theta)|/\hat{\mathcal{Z}}(\theta)$ with $\theta = 2.31, 2.60, 2.83$ and 3.14 in Table VI for various $m(\theta)$. The relative errors $|\delta\hat{\mathcal{Z}}(\theta)|/\hat{\mathcal{Z}}(\theta)$ for $\gamma = 8.0, 10.0$ and 13.0 increase rapidly with θ and exceed 1.0 for $\theta \gtrsim 2.8$. It is seen in Table VI that for $\gamma = 5.0, m_{32/50}(\theta)$ and $m_{38/50}(\theta)$, the images $\hat{\mathcal{Z}}(\theta)$ have small uncertainties.

As seen in (ii), some of the images $\mathcal{Z}^{(\alpha)}(\theta)$ vary over several orders as α varies, and the images $\hat{\mathcal{Z}}(\theta)$ calculated from these $\mathcal{Z}^{(\alpha)}(\theta)$ depend strongly on $g(\alpha)$ for large values of θ . For these images, the relative errors are large. For $\gamma \geq 7.0$, $\hat{\mathcal{Z}}(\theta)$ is such that $\Delta(\theta) > 0.1$ for $\theta \gtrsim \theta_\epsilon$ and $|\delta\hat{\mathcal{Z}}(\theta)|/\hat{\mathcal{Z}}(\theta) > 1.0$. Contrastingly, the other images $\mathcal{Z}^{(\alpha)}(\theta)$ [$\gamma \leq 6.0$ and $m_{L/L_0}(\theta)$] do not vary over the range of integration in Eq. (2.17), and these $\hat{\mathcal{Z}}(\theta)$ are independent of $g(\alpha)$, with $\Delta(\theta) < 0.1$ over the entire range of θ . The relative errors $|\delta\hat{\mathcal{Z}}(\theta)|/\hat{\mathcal{Z}}(\theta)$ for these cases [$\gamma \leq 6.0$ and $m_{L/L_0}(\theta)$] increase with θ but do not exceed 1.0 . This indicates that the uncertainty reflects the prior information dependence of the most probable image.

Summarizing the above analysis, we present the results for $\hat{\mathcal{Z}}(\theta)$ in Fig. 10 for various $m(\theta)$. All the results obtained using the MEM behave smoothly over the entire range of θ . For $\theta \lesssim 2.3$, these eight images fall on the same curve, and the MEM reproduces images consistent with the FTM. For $\theta \gtrsim 2.5$, by contrast, the $m(\theta)$ dependence of $\hat{\mathcal{Z}}(\theta)$ is clearly seen. In the large θ , $\hat{\mathcal{Z}}(\theta)$ for $\gamma = 8.0$ and 13.0 , which possess large errors, decrease over several orders as θ increases, while the other images with small errors gradually decrease as θ increases. Each of these images obtained in Fig. 10 could be a candidate for the true image. With the observation that $\hat{\mathcal{Z}}(\theta)$ depends strongly on $m(\theta)$ in the region where the values of $\hat{\mathcal{Z}}(\theta)$ are smaller than that of ϵ , the $m(\theta)$ dependence of $\hat{\mathcal{Z}}(\theta)$ reflects the flattening phenomenon in the FTM.

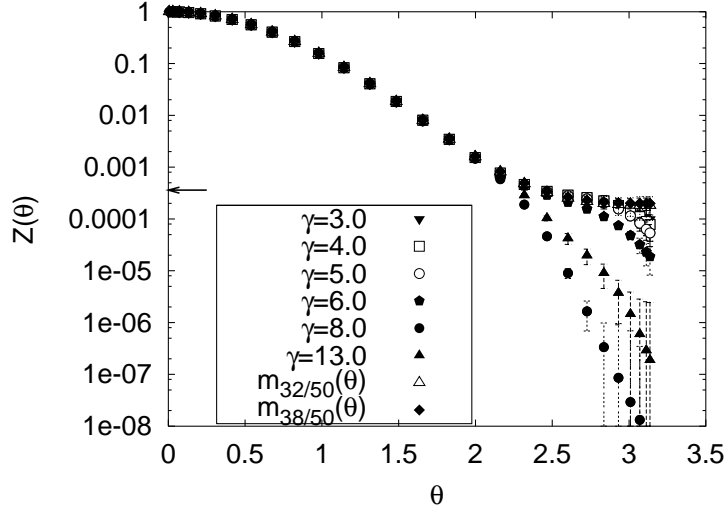


Fig. 10. The most probable images $\hat{Z}(\theta)$ for various $m(\theta)$. The arrow indicates the value of ϵ ($= 3.610 \times 10^{-4}$).

§4. Conclusions and discussion

In this paper, we have applied the MEM to the MC data of the CP^3 model. We have studied how the flattening phenomenon is observed with the MEM. For this purpose, two types of data were used, that for $L = 38$, in which no flattening is observed, and that for $L = 50$, in which flattening is reproduced through the Fourier transform.

The results we obtained in the present study are the following.

1. In the case without flattening, the MEM yielded images $\hat{Z}(\theta)$ that are almost independent of $m(\theta)$ and $g(\alpha)$. The most probable images $\hat{Z}(\theta)$ are in agreement with the result of the FTM within the errors (see Fig. 2 and Table II).
2. In the case with flattening, we have systematically checked (i) the statistical fluctuations of $\hat{Z}(\theta)$, (ii) the $g(\alpha)$ dependence of $\hat{Z}(\theta)$ and (iii) the relative error of $\hat{Z}(\theta)$. We found that the statistical fluctuations of $\hat{Z}(\theta)$ become smaller as the number of measurements increases except near $\theta = \pi$. We also found that $\hat{Z}(\theta)$ with large errors depends strongly on $g(\alpha)$ in the region of large θ , where the $g(\alpha)$ dependence of $\hat{Z}(\theta)$ was estimated using the quantity $\Delta(\theta)$. Our results are summarized in Fig. 10. All the results obtained using the MEM behave smoothly over the entire range of θ . In the region where the value of $\hat{Z}(\theta)$ is larger than or nearly equal to that of ϵ , (specifically $\theta \lesssim 2.3$), final images fall on the same curve, and the MEM reproduces images consistent with the FTM. Contrastingly, in the region where the value of $\hat{Z}(\theta)$ is smaller than that of ϵ , $\hat{Z}(\theta)$ depends strongly on $m(\theta)$. This $m(\theta)$ dependence of $\hat{Z}(\theta)$ reflects the flattening phenomenon. Each of these images obtained in Fig. 10 could be a candidate for the true image.

In the present study, ϵ given by Eq. (3.1) turns out to be an approximate indicator of the influence of the error in $P(Q)$ to $\mathcal{Z}(\theta)$ in both the FTM and MEM cases. As seen in (ii) presented in §3.2.2, $\hat{\mathcal{Z}}(\theta)$ starts to exhibit the $g(\alpha)$ dependence at $\theta = \theta_\epsilon$ for $m_G(\theta)$ with $\gamma \geq 7.0$, where θ_ϵ is defined by $\hat{\mathcal{Z}}(\theta_\epsilon) \simeq \epsilon$, and $\Delta(\theta_\epsilon) \simeq 0.1$ holds. The other default models investigated here satisfy $\Delta(\theta) < 0.1$ for all θ . For these, the $g(\alpha)$ dependence is very weak, even if $\hat{\mathcal{Z}}(\theta) < \epsilon$. It is worthwhile to study the reason for this.

The magnitude of the relative error depends on $m(\theta)$ for large θ (see Fig. 9). At $\theta = \theta_\epsilon$, the FTM gives $|\delta\mathcal{Z}_{\text{Four}}(\theta_\epsilon)|/\mathcal{Z}_{\text{Four}}(\theta_\epsilon) \simeq 0.3$, while $|\delta\hat{\mathcal{Z}}(\theta_\epsilon)|/\hat{\mathcal{Z}}(\theta_\epsilon) \simeq 0.1$ holds in some cases in the MEM; $\hat{\mathcal{Z}}(\theta)$ for $\gamma = 3.0, 4.0, 5.0, 6.0$ and $m_{38/50}(\theta)$. Although $\delta\hat{\mathcal{Z}}(\theta)$ is the uncertainty in the image, it is necessary to elucidate the different manners in which the error in $P(Q)$ affects $\hat{\mathcal{Z}}(\theta)$ and $\mathcal{Z}_{\text{Four}}(\theta)$. When $\hat{\mathcal{Z}}(\theta)$ depends strongly on $m(\theta)$, each $\hat{\mathcal{Z}}(\theta)$ could be a candidate for the true image. If we had proper knowledge about $m(\theta)$ as prior information, we could identify the true image in a probabilistic sense. Such analysis may allow us to clarify the relationship between the default model dependence and the systematic error.

The MEM provides a probabilistic point of view in the study of theories with the sign problem. The canonical approach²⁷⁾ in the study of lattice field theory with a finite density exhibits a formal correspondence to lattice field theory with the θ term. Noting this correspondence, it may be worthwhile to study lattice QCD with a finite density in terms of the MEM from a probabilistic point of view.

Acknowledgements

The authors thank R. Burkhalter for providing his FORTRAN code for the CP^{N-1} model with a fixed point action. We were informed about a work concerning the canonical approach in finite density QCD, by Prof. Ph. de Forcrand. We thank him for calling our attention to the relevant work by him and his collaborator. This work is supported in part by Grants-in-Aid for Scientific Research (C)(2) for the Japan Society for the Promotion of Science (No. 15540249) and the Ministry of Education, Culture, Sports, Science and Technology (Nos. 13135213 and 13135217). Numerical calculations were performed at Computer and Network Center, Saga University.

References

- 1) G. 't Hooft, Nucl. Phys. **B190** [FS3] (1981), 455.
- 2) J. L. Cardy and E. Rabinovici, Nucl. Phys. **B205** [FS5] (1982), 1.
J. L. Cardy, Nucl. Phys. **B205** [FS5] (1982), 17.
- 3) G. Bhanot, E. Rabinovici, N. Seiberg and P. Woit, Nucl. Phys. **B230** [FS10] (1984), 291.
- 4) U. -J. Wiese, Nucl. Phys. **B318** (1989), 153.
- 5) A. S. Hassan, M. Imachi, N. Tsuzuki and H. Yoneyama, Prog. Theor. Phys. **95** (1995), 175.
M. Imachi, S. Kanou and H. Yoneyama, Prog. Theor. Phys. **102** (1999), 653.
- 6) J. C. Plefka and S. Samuel, Phys. Rev. **D56** (1997), 44.
- 7) H. Fukaya and T. Onogi, Phys. Rev. **D68** (2003), 074503; Phys. Rev. **D70** (2004), 054508.
- 8) V. Azcoiti, G. Di Carlo, A. Galante and V. Laliena, Phys. Rev. Lett. **89** (2002), 141601;

- Phys. Rev. **D69** (2004), 056006.
- 9) J. Ambjorn, K. N. Anagnostopoulos, J. Nishimura and J. J. M. Verbaarschot, J. High Energy Phys. **0210** (2002), 062.
 - 10) R. K. Bryan, Eur. Biophys. J. **18** (1990), 165.
 - 11) M. Jarrell and J. E. Gubernatis, Phys. Rep. **269** (1996), 133.
 - 12) M. Asakawa, T. Hatsuda and Y. Nakahara, Prog. Part. Nucl. Phys. **46** (2001), 459.
 - 13) CP-PACS Collaborations, T. Yamazaki et al., Phys. Rev. **D65** (2002), 014501.
 - 14) H. R. Fiebig, Phys. Rev. **D65** (2002), 094512.
 - 15) C. R. Allton, J. E. Clowser, S. J. Hands, J. B. Kogut and C. G. Strouthos, Phys. Rev. **D66** (2002), 094511.
 - 16) N. Ishii and H. Suganuma, Nucl. Phys. **B** (Proc. Suppl.) **129** (2004), 581.
 - 17) A. Macridin, S. P. Doluweera, M. Jarrell and Th. Maier, cond-mat/0410098.
 - 18) K. Sasaki, S. Sasaki and T. Hatsuda, Phys. Lett. **B623** (2005), 208.
 - 19) S. Ejiri and T. Hatsuda, hep-lat/0509119.
 - 20) T. Umeda and H. Matsufuru, hep-lat/0510026.
 - 21) M. Imachi, Y. Shinno and H. Yoneyama, Prog. Theor. Phys. **111** (2004), 387.
 - 22) M. Imachi, Y. Shinno and H. Yoneyama, hep-lat/0506032.
 - 23) B. Berg and M. Lüscher, Nucl. Phys. **B190** [FS3] (1981), 412.
 - 24) M. Karliner, S. R. Sharpe and Y. F. Chang, Nucl. Phys. **B302** (1988), 204.
 - 25) R. Burkhalter, M. Imachi, Y. Shinno and H. Yoneyama, Prog. Theor. Phys. **106** (2001), 613.
 - 26) P. Hasenfratz and F. Niedermayer, Nucl. Phys. **B414** (1994), 785.
 - 27) S. Kratochvila and Ph. de Forcrand, Nucl. Phys. **B** (Proc. Suppl) **140** (2005), 514; hep-lat/0509143.